IOP Conf. Series: Journal of Physics: Conf. Series **821** (2017) 012010 doi:10.1088/1742-6596/821/1/012010

A flamelet model for transcritical LOx/GCH$_4$ flames

Hagen Müller & Michael Pfitzner

Institut für Thermodynamik, Universität der Bundeswehr München, Werner-Heisenberg-Weg 39, 85577 Neubiberg, Germany

E-mail: hagen.mueller@unibw.de

Abstract. This work presents a numerical framework to efficiently simulate methane combustion at supercritical pressures. A LES flamelet approach is adapted to account for real-gas thermodynamics effects which are a prominent feature of flames at near-critical injection conditions. The thermodynamics model is based on the Peng-Robinson equation of state (PR-EoS) in conjunction with a novel volume-translation method to correct deficiencies in the transcritical regime. The resulting formulation is more accurate than standard cubic EoSs without deteriorating their good computational performance. To consistently account for pressure and strain fluctuations in the flamelet model, an additional enthalpy equation is solved along with the transport equations for mixture fraction and mixture fraction variance. The method is validated against available experimental data for a laboratory scale LOx/GCH$_4$ flame at conditions that resemble those in liquid-propellant rocket engines. The LES result is in good agreement with the measured OH* radiation.

Introduction

Todays main stage liquid-propellant rocket engines (LRE) typically operate at supercritical pressures, i.e., at chamber pressures that exceed the critical pressure of the propellants, and at cryogenic injection temperatures. One or both of the propellants are thus injected at near-critical conditions and mixing, ignition and combustion are affected by non-ideal thermodynamic effects. In particular, the thermodynamic- and transport properties, e.g., density, enthalpy, viscosity, are highly non-linear functions of temperature and pressure. Moreover, the experiments of Mayer *et al.* [1, 2] showed that the surface tension between liquid and vapor is diminished at sufficiently high pressures and mixing is characterized by continuous-phase diffusion rather than by two-phase spray atomization. In these diffusion mixing layers, the fluid properties change drastically and the density may vary by two orders of magnitude within a few micrometers.

Such configurations pose a serious challenge for numerical as well as for experimental studies. At the same time, their investigation is important to better understand the involved processes and to develop tools that help in the design of LREs, but also of other high pressure combustion devices, such as novel Diesel motors or gas turbines. The topic received considerable attention in the last decade and several valuable experiments were carried out. Thorough overviews are given, for instance, by Oschwald *et al.* [3] and by Chehroudi [4] focusing on the joint work of the U.S. Air Force Research Laboratory (AFRL) and the German Aerospace Center (DLR) as well as by Habiballah *et al.* [5] focusing on the Mascotte testing facility. Along with the better understanding that has been generated by the experimental efforts, several groups developed models and numerical tools to perform simulations of near-critical mixing and combustion allowing for a detailed view on the flow. Among the first to conduct large-eddy simulations (LES) of supercritical injection was Oefelein and Yang [6] and later Zong *et al.* [7] as well as Oefelein [8]. These studies showed that the accurate treatment of thermodynamic non-idealities are key to obtain

realistic numerical representations. However, accuracy comes at the cost of numerical effort and a compromise has to be made in order to keep the computational effort manageable. Matheis *et al.* [9] identified and compared various volume-translation methods [10, 11] for cubic equations of state (EoS), such as Peng-Robinson (PR) [12] or Soave-Redlich-Kwong (SRK) [13]. These methods have the advantage to improve the predictive quality of cubic EoSs for near-critical conditions without a significant degradation of their good computational performance. In the present work, we employ the volume-translation method of Abudour *et al.* [14] which is based on the work of Chou and Prausnitz [15]. This method has already been used in our previous LES studies of supercritical nitrogen injection [16] as well as of inert coaxial LN_2/GH_2 injection [17].

In the present work, we focus on simulating the injection and combustion of LOx/GCH_4, at the experimental operating conditions of Singla *et al.* [18]. An additional subject that needs to be addressed is the choice of an appropriate combustion model for this configuration. In previous LES studies of this test case, Guézennec *et al.* [19] employed a reduced reaction mechanism accounting for finite-rate chemistry, while Schmitt *et al.* [20] made the assumption of infinitely fast chemistry. This assumption was also made by Cutrone *et al.* [21] as well as by Kim *et al.* [22] who simulated the test case of Singla *et al.* [18] using a Reynolds-averaged Navier-Stokes (RANS) flamelet model. In the present work, we employ the steady laminar flamelet model for LES [23, 24] using a presumed β-shape probability density function (PDF) for the subgrid-scale (SGS) fluctuations. The choice is supported by the comparative study of Zong *et al.* [25], who showed that the flamelet approach performed better than alternative combustion models for a splitter plate configuration at conditions that were similar to those in Singla *et al.'s* experiments. Furthermore, Ribert *et al.* [26] showed that the chemical consumption rates scale as the square-root of pressure. Thus, the assumption that chemical reactions are considerable faster than mixing time scales and the reaction zone is thin , which is a precondition for the flamelet approach, appears to be appropriate for the present high-pressure configuration. This is also supported by Lacaze and Oefelein [27] who investigated the applicability of the flamelet approach for the LES of supercritical LOx/H_2 combustion.

Numerical and physical modeling

LES equations

In LES, only the large-scale turbulent fluctuations are computed while fluctuations on subgrid-scale (SGS) level have to be modeled. The threshold between unresolved and resolved scale is determined by a certain filter width which is the local cell size in the present work. Filtering the Navier-Stokes equations leads to the filtered LES equations for mass, momentum and energy, cf. Garnier *et al.* [28].

As mentioned before, we employ the flamelet concept [24] to avoid the computational cost of solving a complex chemistry kinetics mechanism. The species composition in the flow field is represented by three parameters: the scalar dissipation rate $\tilde{\chi}$, the resolved mixture fraction $\tilde{f}$ and its subgrid variance $\widetilde{f''^2}$. The scalar dissipation is modeled with an algebraic equation, whereas additional transport equations are introduced for the mixture fraction and its variance that are solved along with the filtered Navier-Stokes equations:

$$\frac{\partial\left(\bar{\rho}\tilde{f}\right)}{\partial t}+\frac{\partial\left(\bar{\rho}\tilde{u}_i\tilde{f}\right)}{\partial x_i}=\frac{\partial}{\partial x_i}\left(\left(\frac{\bar{\mu}}{Sc}+\frac{\mu_e}{Sc_t}\right)\frac{\partial\tilde{f}}{\partial x_i}\right), \tag{1}$$

$$\frac{\partial\left(\bar{\rho}\widetilde{f''^2}\right)}{\partial t}+\frac{\partial\left(\bar{\rho}\tilde{u}_i\widetilde{f''^2}\right)}{\partial x_i}=\frac{\partial}{\partial x_i}\left(\left(\frac{\bar{\mu}}{Sc}+\frac{\mu_e}{Sc_t}\right)\frac{\partial\widetilde{f''^2}}{\partial x_i}\right)-2\bar{\rho}\tilde{\chi}+2\left(\frac{\bar{\mu}}{Sc}+\frac{\mu_e}{Sc_t}\right)\left(\frac{\partial\tilde{f}}{\partial x_i}\right)^2, \tag{2}$$

where a bar $\bar{\star}$ denotes the finite-volume filter and a tilde denotes Favre-filtering, i.e., $\tilde{\star}=\overline{\rho\star}/\bar{\rho}$. x_i are Cartesian coordinates, t is the time, $\bar{\rho}$ is the density, $\tilde{u}_i$ is the velocity component in direction i. μ and μ_e are the molecular and the eddy viscosity, respectively.

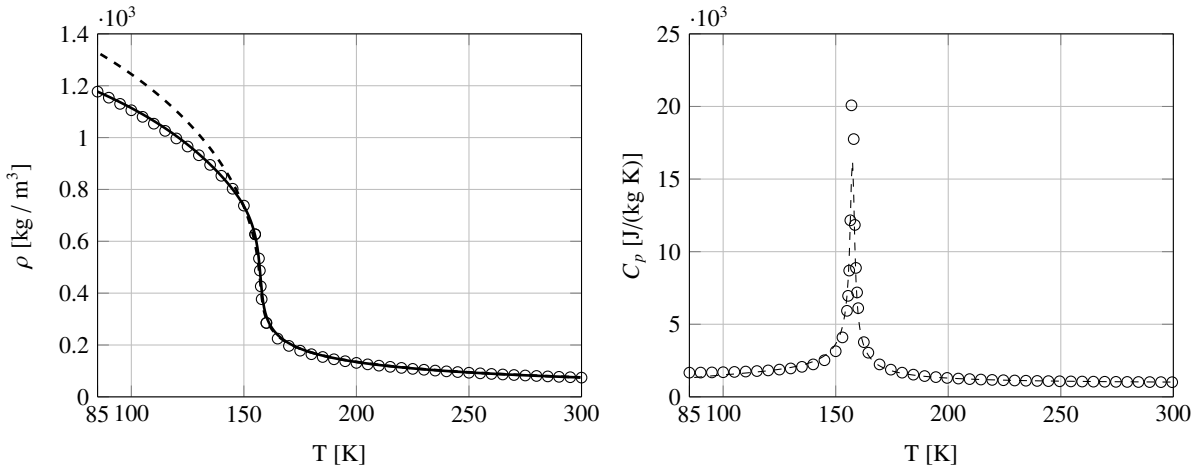

(a) Density (b) Isobaric heat capacity

Figure 1. Verification of the real-gas thermodynamics model for O_2 at $p = 5.61$ MPa: — PR-VTA EoS, −− PR EoS, ∘ NIST chemistry webbook [33].

The eddy viscosity μ_e is calculated using the SGS turbulence model of Vreman [29]. The diffusion of mixture fraction and of mixture fraction variance is modeled using the standard gradient diffusion assumption with the diffusion coefficient being connected with the viscosity through the molecular and turbulent Schmidt number. These are set constant to $Sc = 1.0$ and $Sc_t = 0.7$, respectively. The scalar dissipation rate in Eq. 2 is decomposed into a resolved and a SGS contribution.

$$2\bar{\rho}\tilde{\chi} = 2\frac{\tilde{\mu}}{Sc}\left(\frac{\partial\tilde{f}}{\partial x_i}\right)^2 + C_\chi\frac{\mu_e}{Sc_t}\frac{\widetilde{f''^2}}{\Delta^2} \tag{3}$$

Here, Δ is the local filter size and the model constant C_χ is set to 2.

In the present work, we employ a *Pressure Implicit with Splitting of Operators* (PISO) algorithm [30, 31] for solution of the Navier-Stokes equations. Instead of solving the continuity equation directly, the discretized momentum equation is used to derive a pressure evolution equation, which guarantees mass conservation. This has the advantage that stiff equation systems, especially for low Mach number flows, are avoided and the computation can be run using larger time steps. However, several modifications are necessary to consistently incorporate real-gas thermodynamics models into the standard PISO approach. For details, please see the work of Jarczyk and Pfitzner [32].

Real-gas thermodynamics

The thermodynamic model is based on the mixture PR EoS [12]:

$$p = \frac{RT}{v_{PR} - b_m} - \frac{a_m}{v_{PR}^2 + 2v_{PR}b_m - b_m^2}, \tag{4}$$

where v_{PR} is the molar volume of the mixture, T is the temperature and R is the universal gas constant. Intermolecular attractive forces are described by the temperature dependent function a_m and the reduction of free volume due to the finite volume of the molecules is taken into account by b_m. The mixing rules for these parameters are taken from the work of Harstad *et al.* [10]. The PR EoS is an adequate choice for temperatures above and close to the critical temperature, however, in the transcritical regime considerable deviations from experimental data can be observed [11]. In the present work, we therefore employ the volume-translation method of Abudour *et al.* [14] (PR-VTA), who proposed a generalized form of the

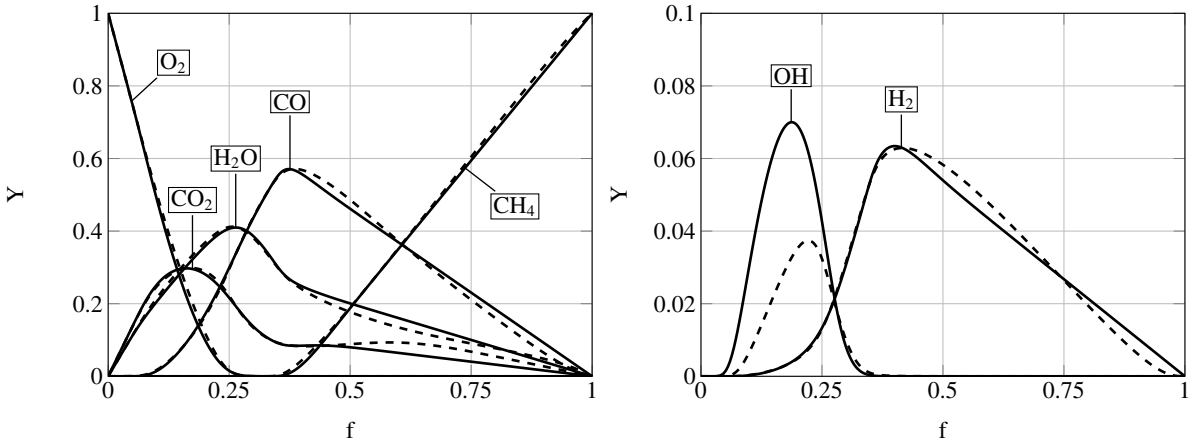

(a) Major species (b) Minor species

Figure 2. CH_4/O_2 flamelet solution for $\chi_{st} \approx 0$ and $p = 5.61$ MPa: —full mechanism (GRI 3.0), −− reduced mechanism of Frassoldati *et al.* [37].

method of Chou and Prausnitz [15] that considerably improves the accuracy of the density prediction at minimal extra computational cost. The basic principle is to shift the thermodynamic state of the fluid along its volume axis keeping pressure and temperature constant.

The caloric properties, e.g. heat capacities and enthalpy, are calculated using the departure function formalism. The quantity of interest is decomposed into an ideal gas contribution, which is calculated at a low reference pressure using NASA polynomials [34], and a pressure-dependent departure function. More details are given, for instance, by Poling *et al.* [35]. The viscosity and the thermal conductivity is modeled using the empirical correlation for dense fluids of Chung *et al.* [36].

The left plot in Figure 1 demonstrates the effect of the volume-translation method on the density prediction for O_2 at $p = 5.61$ MPa. While the uncorrected density deviates from the reference data of the NIST [33] for temperatures below 150 K, the density obtained with PR-VTA is in good agreement with the reference data over the entire temperature range considered in the present work. In particular, for the oxidizer injection condition ($T_{O2} = 85$ K, $p = 5.61$ MPa) of the test case presented later on, the deviation from NIST is 10.33% for the uncorrected PR EoS and only 0.005% for the PR-VTA EoS. The right side of Figure 1 shows the constant pressure heat capacity c_p. Note that only the PR EoS result is shown, since the volume translation of Abudour *et al.* could not be considered in the evaluation of the caloric properties for the reasons mentioned above, cf. Matheis *et al.* [9] for details.

Flamelet model for real fluids

A flamelet model for turbulent non-premixed combustion [23, 24] is employed to cut the cost of solving the chemistry kinetics along with the transport equations. The concept is based on the view of the turbulent flame as an ensemble of thin laminar diffusion flames, generally referred to as flamelets. The underlying assumption is that the characteristic chemical time scales are small compared to the turbulent time scales (high Damköhler number). Another condition for the validity of the flamelet approach is that turbulent vortices do not perturb the inner structure of the flame, i.e. the flame thickness is sufficiently small compared to the turbulent length scales (small turbulent Reynolds number). The main advantage of the flamelet approach is that the flamelets, which describe the local structure of the turbulent flame, are coupled to the turbulent flow by only a few parameters, i.e., the mixture fraction, its variance and the scalar dissipation rate. The chemistry kinetics can thus be handled separately from the turbulent flow. This feature is used to calculate the flamelets in a pre-processing step and store them in look-up tables which are accessed during the LES to retrieve the local species composition.

Table 1. Boundary conditions of Singla *et al.* [18].

LOx			CH_4		
$\dot{m}$ [g/s]	T_{in} [K]	ρ_{in} [kg/m^3]	$\dot{m}$ [g/s]	T_{in} [K]	ρ_{in} [kg/m^3]
44.4	85	1177	143.1	288	42

Flamelet models have often been used for flows at atmospheric pressure where broad experience has been gathered for different flame types. However, the approach needs to be revised when used to simulate combustion at supercritical pressures. The influence of real-gas thermodynamics on the inner structure of the supercritical hydrogen flames has been investigated by several groups [38, 26, 39, 40]. They show that thermodynamic non-idealities have no significant effect on the inner structure of the flame and an ideal gas law is sufficient to calculate the flamelets. The reason is the strong temperature increase near the flame front that limits the influence of real-gas effects to regions close to $f = 0$ and $f = 1$. A further aspect is the influence of pressure on the reaction kinetics. Since the reaction speed increases with the pressure, supercritical flames are shown to be thin and resistant to strain [38, 26]. This supports the flamelet assumptions of high Damköhler number and small turbulent Reynolds number. However, as pointed out by Lacaze and Oefelein [27], an additional energy equation is needed in the LES to account for pressure and strain variations. In particular, the effect of pressure on the flamelet solution is typically neglected in the flamelet calculation. Considering that the caloric properties are pressure-dependent when using the PR EoS, energy conservation can only be guaranteed by solving an additional energy equation in the LES.

In the present work, we use the Flamemaster software of Pitsch [41] to solve the flamelet equations for a strained counterflow diffusion flame configuration under the assumption that the fluid is an ideal gas. The reduced methane oxidation mechanism of Jones and Lindstedt [42] with additional reactions that account for dissociation of water and oxygen as proposed by Frassoldati *et al.* [37] is used to reduce the number of species. The flamelet solution is filtered using a β-shape PDF for the mixture fraction and a Dirac delta function for the PDF of the scalar dissipation rate to account for SGS fluctuations. The filtered species composition is accessed during the LES using the filtered values of mixture fraction, mixture fraction variance and scalar dissipation. The effect of pressure fluctuations and real-gas thermodynamics is thus not reflected in the species composition of the flame structure. However, we solve an enthalpy transport equation and calculate the thermodynamic properties in the LES using the real-gas thermodynamics models based on the volume correction of Abudour *et al.* [14].

Figure 2 shows the result of a CH_4/O_2 flamelet simulation at $\chi_{st} \approx 0$ and $p = 5.61$ MPa. To verify that the simplified reaction mechanism of Frassoldati *et al.* [37] is appropriate for the present configuration, the results are compared with a flamelet simulation using the full CH_4/O_2 reaction mechanism (GRI 3.0 [43]). Only minor differences can be observed for the major species.

Experimental and numerical setup

Reference experiment

The present numerical approach to simulate real-gas combustion is tested against the measurements of Singla *et al.* [18] who performed a series of experiments for trans- and supercritical LOx/CH_4 flames at the Mascotte testing facility. The test bench has previously been used to study high-pressure hydrogen flames [5, 44] and has been extended to allow for the use of methane as fuel. The combustion chamber is a 50×50 mm^2 square duct with a length of 400 mm and a converging-diverging nozzle at the chamber end. The propellants are injected through a single coaxial injector element that is mounted on the faceplate. All four side walls of the chamber can be equipped with rectangular windows to allow for optical measurements. Singla *et al.* [18] have used a intensified (CCD) camera to collect the spontaneous emission of OH^* at a rate of 15 Hz. In addition the CH^* signal has been detected with an ICCD camera at

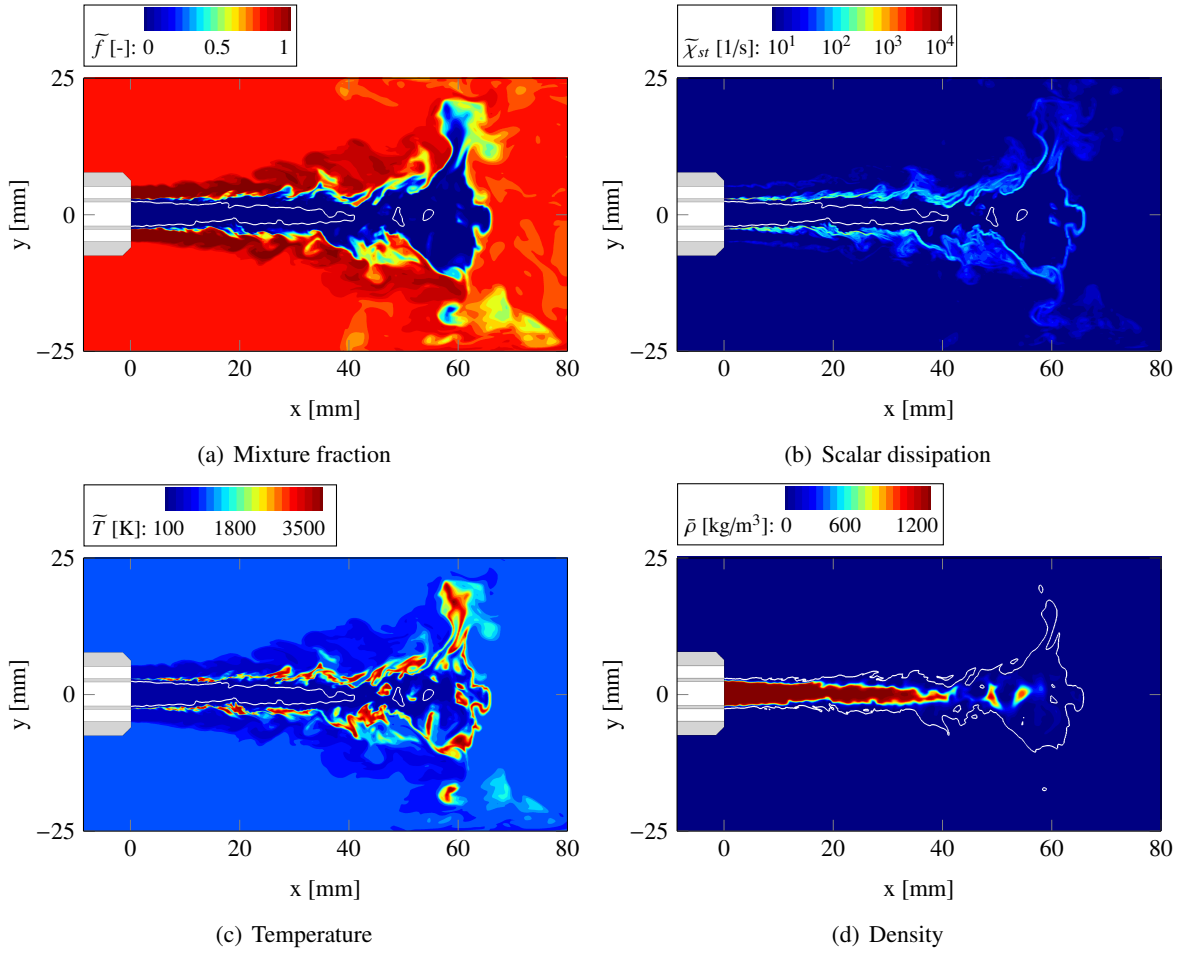

(a) Mixture fraction (b) Scalar dissipation

(c) Temperature (d) Density

Figure 3. Instantaneous fields of mixture fraction, scalar dissipation rate, temperature and density in a plane perpendicular to the inflow plane. The white line in a), b) and c) denotes the pseudo-critical temperature of oxygen $T_{pb,O_2} = 157.4$ K. The white line in d) denotes the stoichiometric mixture $f = 0.2$.

a rate of 2.5 Hz. After averaging the instantaneous images, an Abel transformation has been carried out to obtain slices through the flame which are used for the present comparison with the numerical results.

Singla *et al.* [18] have performed several experiments varying both the chamber pressure and the injection temperature. For the present study, we simulate the operating point G2 for which the injection conditions are summarized in Table 1. The chamber pressure $p = 5.61$ MPa is supercritical with respect to the pure species ($p_{c,O2} = 5.04$ MPa, $p_{c,CH4} = 4.6$ MPa). The temperature of the injected oxygen $T_{O_2} = 85$ K is smaller than the pseudo-critical temperature at these conditions ($T_{pb,O_2} = 157.4$ K) and the fluid is thus in a transcritical state which is characterized by a high liquid-like density and viscosity. However, methane is injected in a purely supercritical state, i.e., both the pressure and the temperature exceed their critical value, and the fluid features a much smaller, gas-like density. The heat release at these conditions is 0.55 MW given that the oxidizer is fully consumed. This is a valid assumption considering that the mass flux ratio $\dot{m}_{O_2}/\dot{m}_{CH_4} = 0.31$ is well below the mass stoichiometric value of 4.

Computational setup

The LES is performed with the open-source CFD software OpenFOAM which has been extended by the real-gas flamelet model described above. The grid comprises 16×10^6 hexahedral cells and is block-structured. The minimal axial and radial cell size at the injector is 0.2 mm and 0.025 mm, respectively.

To reduce the numerical cost, the numerical domain is truncated after 150 mm. This is sufficient to accommodate the flame and avoid interference with the outflow boundary. The inner tube of the coaxial injector is $D = 4.4$ mm and the width of the annulus and the post is $\Delta D_{CH_4} = 2.2$ mm and $\Delta D_p = 0.6$ mm, respectively.

The turbulent inflow data for both the O_2 and the CH_4 inlet are generated with a separate precursor incompressible LES using cyclic boundary conditions in axial direction. The domain length for these simulations is $2\pi D_h$, where D_h is the hydraulic diameter of the respective inflow. Slices of the turbulent velocity fields are extracted from this simulation and accumulated in a database which is then used to interpolate the turbulent velocity field onto the coarser grid of the flame simulation.

For spatial discretization we use a second-order central differences scheme with a van Leer limiter. To avoid unphysical oscillations, it was necessary to use localized artificial dissipation μ^* in regions of high density gradients.

$$\mu^* = C_\mu \, \bar{\rho} \, a_s \, \Delta^2 \left| \frac{\partial Z}{\partial x_j} \right| \tag{5}$$

a_s and Δ are the speed of sound and the local filter width, respectively. The constant C_μ is set to 0.01. The method is similar to that proposed by Terashima *et al.* [45], however, as a sensor we use the local gradient of the compressibility factor ($Z = pv/RT$), which is zero in regions where real gas effects are negligible.

Results

General flame features

To give a qualitative impression of the general features of the flame, Figure 3 shows the instantaneous fields of mixture fraction, scalar dissipation rate, temperature and density. The white line in Figure 3 a), b) and c) denotes the pseudo-critical temperature of oxygen and marks the region of high density gradient. The fluid which is enclosed by this line features high liquid-like densities and a low velocity. The white line in Figure 3 d) denotes the stoichiometric mixture fraction and marks the flame front.

Close to the injector at $x < 15$ mm, a thin diffusion flame can be observed. The flame surface is perturbed by small scale turbulent structures and it exerts a relatively high level of strain. The maximum scalar dissipation rates in this region are in the order of 10^4 s^{-1}. Further downstream the boundary layer instability grows and large scale eddies evolve leading to a higher degree of flame wrinkling and a thickening of the mean flame front. However, the continuous dense oxygen core persists until $x \approx 40$ mm. Thereafter dense pockets of O_2 detach from the core. They are transported further downstream

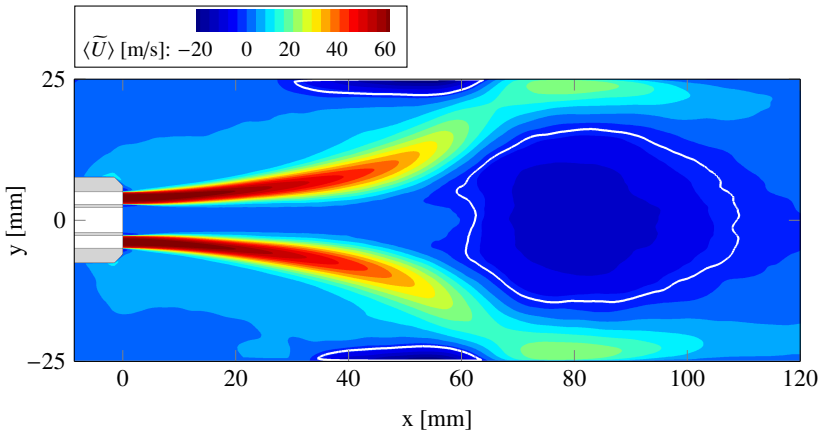

Figure 4. Averaged axial velocity field in a plane perpendicular to the inflow plane. The white line denotes $\langle U \rangle = 0$ m/s.

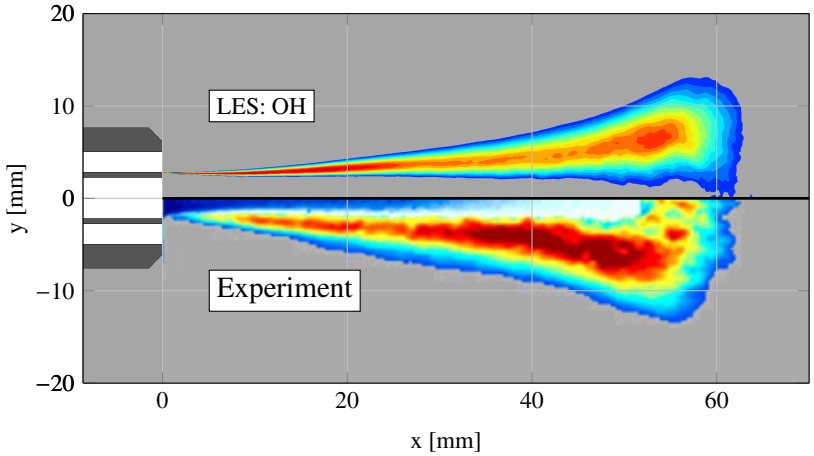

Figure 5. Averaged OH mass fraction in comparison with the measured OH* radiation of Singla *et al.* [18].

where they react with the surrounding fuel. In this region, i.e., at $x \approx 50$ mm, a strong radial expansion can be observed. The flow is redirected towards the chamber wall and reactions stop shortly thereafter at $x \approx 60$ mm.

This characteristic flame shape can be explained considering the averaged velocity field which is shown in Figure 4. The white lines denote zero axial velocity and mark the recirculation zones. In addition to the backflow region that forms close to the chamber wall between the flame and the face plate, a secondary recirculation can be observed downstream of the reaction zone. This was also observed in the LES result of Schmitt *et al.* [20]. Due to the interaction with the chamber wall in the rear part of the flame, the flow of hot combustion products is redirected towards the chamber axis where is flows back towards the flame. The momentum of the backflow further increases the expansion of the flame leading to a stable flow condition.

Comparison with experimental data

Temporal averaging was started after the flow field was considered fully developed in the region of interest and then continued for $\Delta t = 0.08s \approx 45D/\bar{U}_{O_2}$. In addition, we make use of the symmetry and spatially average the flow field using the 4 half planes that are perpendicular to the injector plane and the chamber wall. The averaged OH mass fraction is compared with the experimental result of Singla *et al.* [18] in Figure 5.

The characteristic flame shape, which has been discussed in the previous section, can also be seen in the experimental result. The first section of the flame is characterized by a constant spreading angle. At $x \approx 40$ mm a sudden expansion can be observed, which is followed by an abrupt end of reaction. This is well reproduced by the LES. Also the calculated length of the flame as indicated by the OH mass fraction is in excellent agreement with the measurement.

Conclusion

The current contribution presents a real-gas flamelet model for large-eddy simulations (LES) to simulate non-premixed combustion at supercritical pressures. The main challenges are the accurate modeling of thermodynamic non-idealities as well as their consistent coupling with the flamelet approach. The thermodynamic model used herein consists of a cubic Peng-Robinson equation of state (PR EoS) and a volume-translation method that corrects deficiencies of the PR EoS at low temperatures. This method yields a highly accurate thermal equation of state at reasonable computational effort. Pressure and strain fluctuations are taken into account by solving the energy equation along with the mixture fraction

transport equation which represents the local species composition. Subgrid mixture fraction fluctuations are taken into account with a β-shape probability density function and a reduced methane reaction mechanism that consists of 9 species and 6 reactions is used to generate the flamelets.

Simulations have been performed for the experimental test case of Singla *et al.* [18], in which liquid oxygen and gaseous methane are injected into a rectangular combustion chamber. The pressure is supercritical. A comparison with the available OH^* radiation measurements shows that the predicted flame length is in excellent agreement with the experiment and characteristic flame features are well reproduced. The result indicates that the real-gas adapted flamelet approach for combustion at supercritical pressures that is presented herein is well suited to simulate this flame.

Acknowledgments

The authors gratefully acknowledge the German Research Foundation (Deutsche Forschungsgemeinschaft (DFG)) for providing financial support in the framework of SFB/TRR 40 *Fundamental Technologies for the Development of Future Space-Transport-System Components under High Thermal and Mechanical Loads* and the Gauss Centre for Supercomputing e.V. (www.gauss-centre.eu) for funding this project by providing computing time on the GCS Supercomputer SuperMUC at Leibniz Supercomputing Centre (LRZ, http://www.lrz.de).

References

[1] W. Mayer and H. Tamura, "Propellant injection in a liquid oxygen/gaseous hydrogen rocket engine," *Journal of Propulsion and Power*, vol. 12, no. 6, pp. 1137–1147, 1996.
[2] W. Mayer, A. Schik, B. Vielle, C. Chaveau, I. Gökalp, and D. Talley, "Atomization and breakup of cryogenic propellants under high pressure subcritical and supercritical conditions," *Journal of Propulsion and Power*, vol. 14, no. 5, pp. 835–842, 1998.
[3] M. Oschwald, J. J. Smith, R. Branam, J. Hussong, A. Schik, B. Chehroudi, and D. Talley, "Injection of fluids into supercritical environments," *Combustion Science and Technology*, vol. 178, no. 1-3, pp. 49–100, 2006.
[4] B. Chehroudi, "Recent experimental efforts on high-pressure supercritical injection for liquid rockets and their implications," *International Journal of Aerospace Engineering*, vol. 2012, 2012.
[5] M. Habiballah, M. Orain, F. Grisch, L. Vingert, and P. Gicquel, "Experimental studies of high-pressure cryogenic flames on the Mascotte facility," *Combustion Science and Technology*, vol. 178, no. 1-3, pp. 101–128, 2006.
[6] J. Oefelein and V. Yang, "Modeling high-pressure mixing and combustion processes in liquid rocket engines," *Journal of Propulsion and Power*, vol. 14, no. 5, pp. 843–857, 1998.
[7] N. Zong, H. Meng, S. Y. Hsieh, and V. Yang, "A numerical study of cryogenic fluid injection and mixing under supercritical conditions," *Physics of Fluids (1994-present)*, vol. 16, no. 12, pp. 4248–4261, 2004.
[8] J. Oefelein, "Mixing and combustion of cryogenic oxygen-hydrogen shear-coaxial jet flames at supercritical pressure," *Combustion Science and Technology*, vol. 178, no. 1-3, pp. 229–252, 2006.
[9] J. Matheis, H. Müller, C. Lenz, M. Pfitzner, and S. Hickel, "Volume translation methods for real-gas computational fluid dynamics simulations," *Journal of Supercritical Fluids*, vol. 107, pp. 422–432, 2016.
[10] K. G. Harstad, R. S. Miller, and J. Bellan, "Efficient high-pressure state equations," *AIChE Journal*, vol. 43, no. 6, pp. 1605–1610, 1997.
[11] K. Frey, M. Modell, and J. W. Tester, "Density-and-temperature-dependent volume translation for the SRK EOS: 1. Pure fluid," *Fluid Phase Equilibria*, vol. 279, no. 1, pp. 56–63, 2009.
[12] D.-Y. Peng and D. B. Robinson, "A new two-constant equation of state," *Industrial & Engineering Chemistry Fundamentals*, vol. 15, no. 1, pp. 59–64, 1976.
[13] G. Soave, "Equilibrium constants from a modified Redlich-Kwong equation of state," *Chemical Engineering Science*, vol. 27, no. 6, pp. 1197–1203, 1972.
[14] A. M. Abudour, S. A. Mohammad, R. L. Robinson, and K. A. M. Gasem, "Volume-translated Peng-Robinson equation of state for liquid densities of diverse binary mixtures," *Fluid Phase Equilibria*, vol. 349, pp. 37–55, 2013.
[15] G. F. Chou and J. M. Prausnitz, "A phenomenological correction to an equation of state for the critical region," *AIChE Journal*, vol. 35, no. 9, pp. 1487–1496, 1989.
[16] H. Müller, C. A. Niedermeier, J. Matheis, M. Pfitzner, and S. Hickel, "Large-eddy simulation of nitrogen injection at trans- and supercritical conditions," *Physics of Fluids (1994-present)*, vol. 28, no. 1, p. 15102, 2016.
[17] H. Müller, M. Pfitzner, J. Matheis, and S. Hickel, "Large-Eddy Simulation of coaxial LN2/GH2 injection at trans- and supercritical conditions," *Journal of Propulsion and Power*, vol. 32, no. 1, pp. 46–56, 2016.
[18] G. Singla, P. Scouflaire, C. Rolon, and S. Candel, "Transcritical oxygen/transcritical or supercritical methane combustion.," in *Proceedings of the Combustion Institute*, vol. 30, pp. 2921–2928, 2005.

[19] N. Guezennec, M. Masquelet, and S. Menon, "Large Eddy Simulation of flame-turbulence interactions in a LOX-CH4 shear coaxial injector," in *50th AIAA Aerospace Sciences Meeting including the New Horizons Forum and Aerospace Exposition: AIAA paper 2012-1267*, 2012.
[20] T. Schmitt, Y. Méry, M. Boileau, and S. Candel, "Large-eddy simulation of oxygen/methane flames under transcritical conditions," in *Proceedings of the Combustion Institute*, vol. 33, pp. 1383–1390, 2011.
[21] L. Cutrone, P. De Palma, G. Pascazio, and M. Napolitano, "A RANS flamelet-progress-variable method for computing reacting flows of real-gas mixtures," *Computers and Fluids*, vol. 39, no. 3, pp. 485–498, 2010.
[22] T. Kim, Y. Kim, and S. K. Kim, "Effects of pressure and inlet temperature on coaxial gaseous methane/liquid oxygen turbulent jet flame under transcritical conditions," *Journal of Supercritical Fluids*, vol. 81, pp. 164–174, 2013.
[23] N. Peters, "Laminar diffusion flamelet models in non-premixed turbulent combustion," *Progress in Energy and Combustion Science*, vol. 10, no. 3, pp. 319–339, 1984.
[24] N. Peters, *Turbulent combustion*. Cambridge University Press, 2000.
[25] N. Zong, G. Ribert, and V. Yang, "A flamelet approach for modeling of liquid oxygen (LOX)/methane flames at supercritical pressures," in *46th AIAA Aerospace Sciences Meeting and Exhibit: AIAA paper 2008-946*, 2008.
[26] G. Ribert, N. Zong, V. Yang, L. Pons, N. Darabiha, and S. Candel, "Counterflow diffusion flames of general fluids: Oxygen/hydrogen mixtures," *Combustion and Flame*, vol. 154, no. 3, pp. 319–330, 2008.
[27] G. Lacaze and J. C. Oefelein, "A non-premixed combustion model based on flame structure analysis at supercritical pressures," *Combustion and Flame*, vol. 159, no. 6, pp. 2087–2103, 2012.
[28] E. Garnier, N. A. Adams, and P. Sagaut, *Large eddy simulation for compressible flows*. Springer, 2009.
[29] A. W. Vreman, "An eddy-viscosity subgrid-scale model for turbulent shear flow: Algebraic theory and applications," *Physics of Fluids (1994 - present)*, vol. 16, no. 10, pp. 3670–3681, 2004.
[30] R. I. Issa, "Solution of the implicitly discretised fluid flow equations by operator-splitting," *Journal of Computational Physics*, vol. 62, no. 1, pp. 40–65, 1985.
[31] R. I. Issa, "Solution of the implicitly discretised reacting flow equations by operator-splitting," *Journal of Computational Physics*, vol. 93, no. 2, pp. 388–410, 1991.
[32] M. Jarczyk and M. Pfitzner, "Large Eddy Simulation of supercritical nitrogen jets," in *50th AIAA Aerospace Sciences Meeting including the New Horizons Forum and Aerospace Exposition: AIAA paper 2012-1270*, 2012.
[33] "National Institute of Standards and Technology."
[34] E. Goos, A. Burcat, and B. Ruscic, "Extended third millennium ideal gas and condensed phase thermochemical database for combustion with updates from active thermochemical tables," 2009.
[35] B. E. Poling, J. M. Prausnitz, and J. P. O'Connell, *The properties of gases and liquids*. Mc Graw Hill, 2001.
[36] T.-H. Chung, M. Ajlan, L. L. Lee, and K. E. Starling, "Generalized multiparameter correlation for nonpolar and polar fluid transport properties," *Industrial & Engineering Chemistry Research*, vol. 27, no. 4, pp. 671–679, 1988.
[37] A. Frassoldati, A. Cuoci, T. Faravelli, E. Ranzi, C. Candusso, and D. Tolazzi, "Simplified kinetic schemes for oxy-fuel combustion," in *1st International Conference on Sustainable Fossil Fuels for Future Energy*, pp. 6–10, 2009.
[38] L. Pons, N. Darabiha, S. Candel, G. Ribert, and V. Yang, "Mass transfer and combustion in transcritical non-premixed counterflows," *Combustion Theory and Modelling*, vol. 13, no. 1, pp. 57–81, 2009.
[39] S. Pohl, M. Jarczyk, M. Pfitzner, and B. Rogg, "Real gas CFD simulations of hydrogen/oxygen supercritical combustion," in *Progress in Propulsion Physics*, vol. 4, pp. 583–614, EDP Sciences, 2013.
[40] T. Kim, Y. Kim, and S.-K. Kim, "Real-fluid flamelet modeling for gaseous hydrogen/cryogenic liquid oxygen jet flames at supercritical pressure," *Journal of Supercritical Fluids*, vol. 58, no. 2, pp. 254–262, 2011.
[41] H. Pitsch, "Flamemaster."
[42] W. Jones and R. Lindstedt, "Global reaction schemes for hydrocarbon combustion," *Combustion and Flame*, vol. 73, no. 3, pp. 233–249, 1988.
[43] G. P. Smith, D. M. Golden, M. Frenklach, N. W. Moriarty, B. Eiteneer, M. Goldenberg, C. T. Bowman, R. K. Hanson, S. Song, W. C. Gardiner, V. V. Lissianski, and Z. Qin, "Gas Research Institute."
[44] S. Candel, G. Herding, R. Snyder, P. Scouflaire, C. Rolon, L. Vingert, M. Habiballah, F. Grisch, M. Péalat, P. Bouchardy, D. Stepowski, A. Cessou, and P. Colin, "Experimental investigation of shear coaxial cryogenic jet flames," *Journal of Propulsion and Power*, vol. 14, no. 5, pp. 826–834, 1998.
[45] H. Terashima, S. Kawai, and N. Yamanishi, "High-resolution numerical method for supercritical flows with large density variations," *AIAA Journal*, vol. 49, no. 12, pp. 2658–2672, 2011.